Title

Pore-forming activity of S. pneumoniae pneumolysin disrupts the paracellular localization of the epithelial adherens junction protein E-cadherin

Permalink

https://escholarship.org/uc/item/2tv1q28j

Journal

Infection and Immunity, 91(9)

ISSN

0019-9567

Authors

Xu, Shuying

Mo, Devons

Rizvi, Fatima Z

et al.

Publication Date

2023-09-14

DOI

10.1128/iai.00213-23

Copyright Information

Peer reviewed

Pore-forming activity of *S. pneumoniae* pneumolysin disrupts the paracellular localization of the epithelial adherens junction protein E-cadherin

Shuying Xu,[1,2] Devons Mo,[3,4] Fatima Z. Rizvi,[3,4] Juan P. Rosa,[1,5] Jorge Ruiz,[1,6] Shumin Tan,[1] Rodney K. Tweten,[7] John M. Leong,[1,8] Walter Adams[1,3]

AUTHOR AFFILIATIONS See affiliation list on p. 16.

ABSTRACT *Streptococcus pneumoniae,* a common cause of community-acquired bacterial pneumonia, can cross the respiratory epithelial barrier to cause lethal septicemia and meningitis. *S. pneumoniae* pore-forming toxin pneumolysin (PLY) triggers robust neutrophil (PMN) infiltration that promotes bacterial transepithelial migration *in vitro* and disseminated disease in mice. Apical infection of polarized respiratory epithelial monolayers by *S. pneumoniae* at a multiplicity of infection (MOI) of 20 resulted in recruitment of PMNs, loss of 50% of the monolayer, and PMN-dependent bacterial translocation. Reducing the MOI to 2 decreased PMN recruitment two-fold and preserved the monolayer, but apical-to-basolateral translocation of *S. pneumoniae* remained relatively efficient. At both MOI of 2 and 20, PLY was required for maximal PMN recruitment and bacterial translocation. Co-infection by wild-type *S. pneumoniae* restored translocation by a PLY-deficient mutant, indicating that PLY can act in *trans*. Investigating the contribution of *S. pneumoniae* infection on apical junction complexes in the absence of PMN transmigration, we found that *S. pneumoniae* infection triggered the cleavage and mislocalization of the adherens junction (AJ) protein E-cadherin. This disruption was PLY-dependent at MOI of 2 and was recapitulated by purified PLY, requiring its pore-forming activity. In contrast, at MOI of 20, E-cadherin disruption was independent of PLY, indicating that *S. pneumoniae* encodes multiple means to disrupt epithelial integrity. This disruption was insufficient to promote bacterial translocation in the absence of PMNs. Thus, *S. pneumoniae* triggers cleavage and mislocalization of E-cadherin through PLY-dependent and -independent mechanisms, but maximal bacterial translocation across epithelial monolayers requires PLY-dependent neutrophil transmigration.

KEYWORDS neutrophils, epithelial cell junction, E-cadherin, airway mucosal barrier, cholesterol-dependent cytolysin

*S*treptococcus pneumoniae (the pneumococcus, or SPN) is the most frequently isolated causative pathogen of pneumonia, with over 150,000 hospitalizations annually in the United States alone and a mortality rate of 5–7% (1). An ominous development in the course of pneumococcal disease is the translocation of bacteria from the lung into the bloodstream. Indeed, the case fatality rate of pneumococcal disease increases to 15–20% upon development of bacteremia (2). The respiratory epithelium, like other mucosal surfaces, serves as a first line of defense against invading pathogens by maintaining a physical barrier comprised of tight junction (TJ) and adherens junction (AJ) multiprotein complexes (3). TJ proteins, such as scaffolding proteins zonula occludens (ZO) and transmembrane proteins claudins, occludins, and junctional adhesion molecules (JAM), localize to the apical region of cell-cell junctions (4) where they form an intercellular

membrane fence (5). AJ proteins, such as E-cadherin and catenins, are located basolateral to TJs and are essential for the formation and maturation of cell-cell contacts (6). Orchestration of junction protein abundance, localization, coupling to the cytoskeleton, and interaction with multiple cellular signaling pathways are all essential for effective epithelial barrier function (3).

Models for pneumonia and for other pulmonary diseases such as acute lung injury, asthma, and acute respiratory distress syndrome feature loss of pulmonary epithelial integrity and concomitant deleterious outcome (7, 8). Indeed, *S. pneumoniae* infection reduces epithelial junction organization in explanted human lung tissue (4), and murine models suggest that *S. pneumoniae* modulates airway epithelial junctions, influencing the degree of paracellular bacterial migration (9, 10). *S. pneumoniae* pneumolysin (PLY), a major *S. pneumoniae* virulence factor that belongs to cholesterol-dependent cytolysins (CDCs), which form ~25 nm diameter pores in mammalian cell membranes, may play a critical role in this process. Pore formation by CDCs activates cytoskeletal rearrangement (11) and calcium flux (12), two processes that can lead to the breakdown of cellular junctions. Two separate studies have implicated PLY in damaging TJs (13, 14), such as ZO-1. In addition, other *S. pneumoniae* factors have been reported to downregulate TJ components, such as TLR stimulants (9) and pneumococcal neuraminidase (15).

A hallmark of *S. pneumoniae* lung infection is the massive influx of neutrophils (polymorphonuclear leukocytes, or PMNs) into airspaces (16, 17), and in addition to directly disrupting epithelial integrity, PLY is a potent activator of inflammation. PLY triggers the production of neutrophil chemoattractants (18, 19), including epithelial production of the eicosanoid hepoxilin A3 (HXA_3), resulting in PMN transepithelial migration (20, 21). Intranasal and intratracheal challenge of mice with *S. pneumoniae* has demonstrated an important role for PMNs in the clearance of pneumococci early in the infection (17, 22), in part reflecting their diverse range of anti-pneumococcal effector mechanisms such as the production of reactive oxygen species (ROS), proteases and antimicrobial peptides, and neutrophil extracellular traps (17, 23–25). However, these same effector molecules can damage intercellular junctions and increase epithelial permeability (26–28), with prolonged inflammatory PMN responses leading to epithelial barrier disruption, pulmonary edema, and significant lung damage (29, 30). In some mouse models, retention of high numbers of pulmonary PMNs after the initial acute infection stage is associated with bacteremia and lethality, indicating that inappropriate PMN responses exacerbate pneumococcal disease (21, 22). For example, upon pneumococcal lung challenge in mice, diminishing PMN pulmonary infiltration by blocking HXA_3 production effectively decreased bacteremia and promoted 100% survival of an otherwise uniformly fatal infection (21, 31).

The impact of these diverse PLY functions is reflected in the observation that in several pulmonary infection mouse models, PLY is required for maximal inflammation, tissue damage, and bacteremia (32–34). Although the majority of the known effects of PLY on host cells is linked to PLY's pore-forming activity (35), PLY interacts with non-cholesterol receptors such as the mannose receptor C type 1 (MRC-1) on macrophages and dendritic cells (36) and is capable of altering functions of both immune and non-immune cells at sub-cytolytic concentrations (37). In addition, PLY-deficient strains are capable of causing bacteremia (38), suggesting that *S. pneumoniae* encodes multiple factors that contribute to bacterial dissemination. Here, we subjected polarized respiratory epithelial monolayers to apical infection by *S. pneumoniae* and systematically examined the role of infectious dose, PLY-mediated pore formation, and PMN transmigration on the integrity and organization of the AJ protein E-cadherin, as well as on bacterial translocation.

MATERIALS AND METHODS

Bacterial strains and growth conditions

Mid-exponential growth phase aliquots of *S. pneumoniae* TIGR4 (serotype 4) were grown in Todd-Hewitt broth (BD Biosciences) supplemented with 0.5% yeast extract in 5% CO_2 and Oxyrase (Oxyrase, Mansfield, OH), and frozen in growth media with 20% (v/v) glycerol. Bacterial titers in aliquots were confirmed by plating serial dilutions on tryptic soy agar plates supplemented with 5% sheep blood agar (Northeast Laboratory Services, Winslow, ME). The TIGR4 PLY-deficient mutant (Δ*ply*) and GFP-expressing WT and Δ*ply* TIGR4 were gifts from Dr. Andrew Camilli (Tufts University, Boston, MA). The cholesterol-binding activity-deficient PLY mutant (CBS) was generated by transformation of wild-type TIGR4 with linear CBS DNA amplified from *Escherichia coli* plasmid gifted by Dr. Rod Tweten (University of Oklahoma, OH), and screened for non-hemolytic transformants. Insertion of the CBS *ply* gene at the original locus was confirmed by sequencing. For experiments, *S. pneumoniae* strains were grown in Todd-Hewitt broth (BD Biosciences), supplemented with 0.5% yeast extract and Oxyrase, in 5% CO_2 at 37°C and used at mid-log phase to late log phase.

Growth and maintenance of epithelial cells

Human pulmonary mucoepidermoid carcinoma-derived NCI-H292 (H292) cells were grown on the underside of collagen-coated Transwell filters (5 µm pore size, 0.33 cm^2, Corning Life Sciences) in RPMI 1640 medium (American Type Culture Collection, Manassas, VA) supplemented with 2 mM L-glutamine, 10% FBS, and 100 U penicillin/streptomycin.

Preparation and assessment of polarized H292 monolayers

Polarized H292 monolayers were prepared as previously described (39). The transepithelial resistance of lung epithelial monolayers is typically very low (unpublished data). Hence, to assess the generation of intact, confluent H292 monolayers, for a sampling of polarized monolayers, we measured the ability of horseradish peroxidase (HRP) added to the basolateral compartment to be detected in the apical chamber after 20 min, as previously described (40). Potential defects in Transwell monolayer integrity were assessed after collagen coating via detecting excessive buffer loss and after cell seeding via changes in pH of cell media. Approximately 3% of H292 monolayers were excluded from our experiments.

Toxin purification

The expression and purification of recombinant toxins and toxin derivatives from *E. coli* were carried out as previously described (41) with the following modifications. Growth of *E. coli* XL-1 Blue containing pRT20 or derivatives thereof was initiated by inoculating 1 L of sterile TB broth with a 1:100 inoculum of an overnight culture grown at room temperature with 100 µg/mL ampicillin. The 1 L culture was incubated at 37°C with shaking at 200 rpm. At OD_{600} 0.5–0.6, expression of toxin was induced by the addition of isopropyl β-D-thiogalactopyranoside (IPTG, Fisher Scientific) to a final concentration of 1 mM. Ampicillin was also added to a final concentration of 100 µg/mL. The induced culture was grown overnight at room temperature and pelleted by centrifugation. Cell pellets were resuspended in a total of 30 mL of PBS. Halt Protease Inhibitor Cocktail (Thermo Fisher Scientific) was added to prevent proteolytic degradation of the toxin. Cells were lysed by two passages through a microfluidizer, and cell debris was removed by centrifugation at 10,000× *g* for 30 min at 4°C. The supernatant containing the polyhistidine-tagged toxin was loaded onto a Ni-NTA agarose column (Qiagen). The column was then washed with a 20–120 mM gradient of imidazole to remove additional contaminating proteins. Bound toxin was then eluted (2 mL/min) with 10 mL of PBS containing 500 mM imidazole. SDS-PAGE was performed on the collected

fractions to confirm toxin purity. 10% (v/v) glycerol and 5 µM Tris(2-carboxyethyl)phosphine hydrochloride (TCEP) were added to toxin-containing fractions, which were then flash-frozen and stored at −80°C until use.

Toxin activity and cell viability by FACS

Toxin aliquots were thawed on ice and then spun at 14,000 rpm in a microcentrifuge at 4°C to remove protein precipitate for 10 min. Toxin concentration was determined using Bradford Reagent (BioRad) per the manufacturer's instructions. 5×10^5 H292 cells were placed in 100 µL volumes in a non-adherent 96 well plate and were treated for 15 min at 37°C with toxin at varying concentrations for activity determination, or with *S. pneumoniae* at multiplicity of infection (MOI) of 2 or 20 to assess the effect of bacterial infection on membrane permeability. Addition of 5% Triton-X 100 and Hanks' balanced salt solution (HBSS)+ were used as positive and negative lysis controls, respectively. For PMN viability assessment, 5×10^5 human peripheral blood PMNs were plated per well instead. The plate was then spun at 1200 rpm for 5 min and cells were resuspended in 1 mg/mL of propidium iodide (PI). Cells were filtered through 100 µm filters into 100 µL of PBS with 10% serum, placed on ice, and kept in the dark until analysis by flow cytometry. Cells were run through a FACSCalibur flow cytometer (BD Biosciences) and a minimum of 5×10^4 events were analyzed per replicate. For determining toxin activity unit, collected data were analyzed using FlowJo software (Tree Star, Inc.) to determine the toxin concentration that resulted in 50% of the H292 cells becoming PI+. This concentration was defined as "1 Unit" of toxin activity.

Infection and toxin treatment of polarized H292 monolayers

S. pneumoniae grown to log phase were washed and resuspended to indicated concentrations in HBSS supplemented with Ca^{2+} and Mg^{2+}. 25 µL of bacterial suspension was added to the apical surface of inverted Transwells and incubated at 37°C with 5% CO_2 for 2.5 h to allow for attachment and infection of monolayers. To assess for bacterial adhesion, monolayers were infected with GFP-expressing *S. pneumoniae* for 2.5 h then fixed in 4% PFA. Adhered bacteria were visualized by IF microscopy, and bound bacteria per field of view were used to determine total bound bacteria per monolayer. For toxin treatments, 50 µL of the indicated units of toxin were added to the apical surface of inverted Transwells for 1 h and incubated at 37°C with 5% CO_2. After treatment, Transwells were washed and placed in 24-well plates containing HBSS+Ca^{2+}/Mg^{2+} and incubated for an additional 2.5 h to allow for bacteria translocation. Permeability to HRP was used to assess monolayer barrier integrity post treatment. Buffer in the basolateral chambers were sampled and bacterial translocation across the monolayer was evaluated by serial dilutions and plating on blood agar. Bacterial translocation index was calculated as total colony forming units (CFUs) in basolateral chamber normalized to the initial inoculum.

PMN transepithelial migration assay

1×10^6 PMNs, isolated from whole blood obtained from healthy human volunteers, were added to the basolateral chamber after infection of the monolayer with *S. pneumoniae* and allowed to transmigrate for 2.5 h. PMNs in the apical chamber were quantified by myeloperoxidase (MPO) assay, as described (42). Briefly, monolayers and their underlying Transwell filters were removed from individual wells of a 24-well plate, leaving the 24-well plate containing the apical buffer and migrated neutrophils for each sample and control well. To assess viability of transmigrated PMNs in the apical chamber, 20 µL of apical chamber buffer was sampled and incubated with 3,3′,5,5′-tetramethylbenzidine (TMB) substrate for detection of released MPO activity. Then, 50 µL of 10% Triton X-100 was added to the apical chamber and gently rocked for 20 min at 4°C to lyse all transmigrated PMNs. 50 µL of citrate buffer was added to each sample and the 24-well plate was gently rocked for 20 min at

4°C. 2,2′-azino-bis(3-ethylbenzothiazoline-6-sulfonic acid) (ABTS) solution was freshly prepared and 50 µL of hydrogen peroxide was added to it. 100 µL from each well was transferred to a 96-well plate and 100 µL of ABTS solution was added to each sample in the 96-well plate. The 96-well plate was incubated in the dark at room temperature for 5–10 min until it was read on a microplate reader for absorbance at a wavelength of 405 nm. Absorbance measurement was converted to neutrophil number using a standard curve and used to determine percent PMN transmigrated.

Fluorescence microscopy assessment of monolayer viability and integrity

Monolayer viability and integrity were assessed by fluorescence microscopy of DAPI for cell confluency, E-cadherin for AJ organization, and PI for cell permeabilization. To prepare samples for fluorescence microscopy, monolayers were fixed in 4% PFA and stained with 1 mg/mL PI. Another set of fixed monolayers was permeabilized with 0.1% Triton-X 100 in PBS plus 3% BSA, and stained with DAPI, phalloidin, and anti-E-cadherin (24E10), followed by α-rabbit-FITC secondary antibody, and visualized on excised filters. To visualize cell surface-exposed E-cadherin, monolayers were stained with ectodomain E-cadherin antibody (DCMA-1) followed by α-rat-FITC secondary antibody, and then permeabilized with 0.1% Triton-X 100 in PBS plus 3% BSA and stained with DAPI (blue) and phalloidin (red). Quantification of E-cadherin junction organization was carried out with the python script intercellular junction organization quantification (IJOQ) as previously described (43). Briefly, the script quantifies spatial distribution of a junctional molecule along the continuous contacts with neighboring cells by determining the degree of intersection between networks of the molecule to a predefined grid-like network. Percentage epithelial cell loss was quantitated by count of DAPI-stained epithelial cell nuclei per field of view.

Western blot

Transwell monolayers were washed three times in HBSS, excised, and lysed in 100 µL of Pierce radioimmunoprecipitation assay (RIPA) buffer (Thermo Fisher Scientific) containing protease inhibitors (cOmplete Mini; Roche Diagnostics, Indianapolis, IN). Proteins were resolved by SDS-PAGE under reduced conditions and transferred onto a polyvinylidene difluoride (PVDF) membrane for immunoblotting. Membranes were blocked in Tris-buffered saline–1% Tween (TBS-T) with 5% nonfat milk, and subsequently incubated with the E-cadherin antibody (24E10) at 1:1,000. Following washing, immunoblots were probed with the appropriate secondary α-rabbit antibody conjugated to HRP at a dilution of 1:5,000. Immune complexes were detected using the SuperSignal West Pico Chemiluminescent Substrate (ThermoFisher Scientific), following the manufacturer's instructions, and imaged using a Syngene G:Box XR5 imager. Densitometry analysis was carried out with ImageJ FIJI, normalized to the respective beta actin loading control.

Matrix metalloprotease activity

PLY-treated H292 monolayers or PMNs in suspension were treated with 1U PLY and incubated for 30 min at 37°C with 10 µM fluorogenic peptide matrix metalloprotease (MMP) substrate (Mca-PLAQAV-Dpa-RSSSR-NH2, R&D Systems) diluted in 25 mM Tris buffer, pH 8.0. Fluorescence intensity over time was read on a BioTek Synergy HT plate reader and area under the curve of kinetic substrate conversion was used to determine MMP activity.

Presentation of data and statistical analyses

Due to intrinsic donor-to-donor variability of human PMNs and their transmigration, efficiency of transmigration was compared within individual experiments but not between experiments. The conclusions drawn were those found to be reproducible and statistically significant across independent experiments. Statistical analysis was carried out using the program GraphPad Prism (GraphPad Software, San Diego, CA). P-values <

0.05 were considered significant in all cases. For all graphs, the mean values ± SEM are shown.

RESULTS

High-dose *S. pneumoniae* infection elicits PLY-dependent PMN recruitment, which promotes epithelial detachment and bacterial translocation.

Previously, we reported that PMN transmigration is required for retrograde translocation of *S. pneumoniae* across polarized airway epithelial monolayers *in vitro* and for bacteremia in mice (21, 31). We further showed that PMN transmigration is promoted by PLY-induced secretion of the inflammatory eicosanoid HXA_3 (20). Here, we utilized polarized H292 cells grown on 5 µm pore size Transwell filters to directly test whether PLY-promoted PMN transmigration promotes barrier disruption and subsequent bacterial translocation. We first infected monolayers apically with TIGR4 at a calculated MOI of 20 using 1×10^7 total bacteria per Transwell (see Materials and Methods), an infectious dose used in previous reports (20, 21). This resulted in 5×10^5 total bound bacteria per Transwell with indistinguishable binding efficiency between wild-type (WT) TIGR4 and PLY-deficient TIGR4*Δply*, as visualized by immunofluorescence (IF) microscopy (Fig. S1A). Infection with WT TIGR4 triggered the basolateral-to-apical transmigration of $\sim 30 \times 10^4$ human PMNs, accounting for 30% of PMNs added to the basolateral chamber (Fig. 1A, "WT"). This induction of PMN transmigration was partially PLY-dependent, as the TIGR4*Δply* strain was associated with a ~ 1.5-fold reduction in PMN movement compared to the WT strain ($P < 0.01$) (Fig. 1A, "*Δply*"). Nevertheless, the level of TIGR4*Δply*-induced PMN transmigration was 14-fold ($P < 0.0001$) above the mock-infected background level, confirming that PMN transmigration can be elicited in PLY-dependent and -independent manners (21, 31).

To examine the influence of PLY-dependent and -independent PMN transmigration on barrier dysfunction, we measured the apical-to-basolateral flux of HRP and the apical-to-basolateral movement of bacteria. Infection by WT TIGR4 in the presence of PMNs was associated with a three-fold increase in HRP flux ($P < 0.001$) (Fig. 1B, "WT") and the detection of 4.8×10^6 *S. pneumoniae* in the basolateral chamber by quantitation of CFUs ($P < 0.0001$) (Fig. 1C, "WT"), which was approximately 7000-fold more than the number of translocated bacteria in the absence of PMNs (Fig. 1C, "No PMNs," "WT"). The WT TIGR4 translocation index, defined as the number of bacteria in the basolateral chamber at 5 h (2.5h infection followed by 2.5h of PMN co-incubation) post-infection divided by the initial inoculum, was 4.8 in the presence of PMNs, as opposed to ~0.0007 in the absence of PMNs (Fig. 1C), indicating efficient translocation only in the presence of PMNs, consistent with our previous findings (21, 31). (The calculated translocation index of greater than 1 indicates that there is some degree of bacterial replication during the 5 h incubation). Infection with TIGR4*Δply*, which elicited ~1.5-fold less PMN migration than WT TIGR4 (Fig. 1A), led to an equivalently lower level of HRP flux, but this difference did not reach statistical significance (Fig. 1B). The degree of HRP flux induced by TIGR4*Δply* was two-fold greater than baseline HRP flux in mock-infected monolayers, but this difference also did not reach statistical significance (Fig. 1B). Barrier disruption by PMNs in response to TIGR4*Δply* infection was most clearly revealed by bacterial translocation, because 10×10^6 TIGR4*Δply* were present in the basolateral chamber, resulting in a translocation index of 1, and an approximately 1000-fold increase in bacterial transmigration in comparison to that in the absence of PMNs (Fig. 1C). Thus, PMN transmigration, whether induced in a PLY-dependent or -independent manner, promotes *S. pneumoniae* transmigration.

To visualize how PMN transmigration to *S. pneumoniae* disrupted the epithelial barrier, we assessed monolayer confluency after *S. pneumoniae* infection and PMN transmigration by IF staining of host cell nuclei (DAPI) and F-actin (phalloidin). At an MOI of 20, infection by WT TIGR4 or TIGR4*Δply* did not alter monolayer confluency (Fig. 1D, top row), but did result in approximately 50% of cells becoming permeable to PI upon WT TIGR4 infection (Fig. S1B). TIGR4*Δply* infection, on the other hand, did not result in
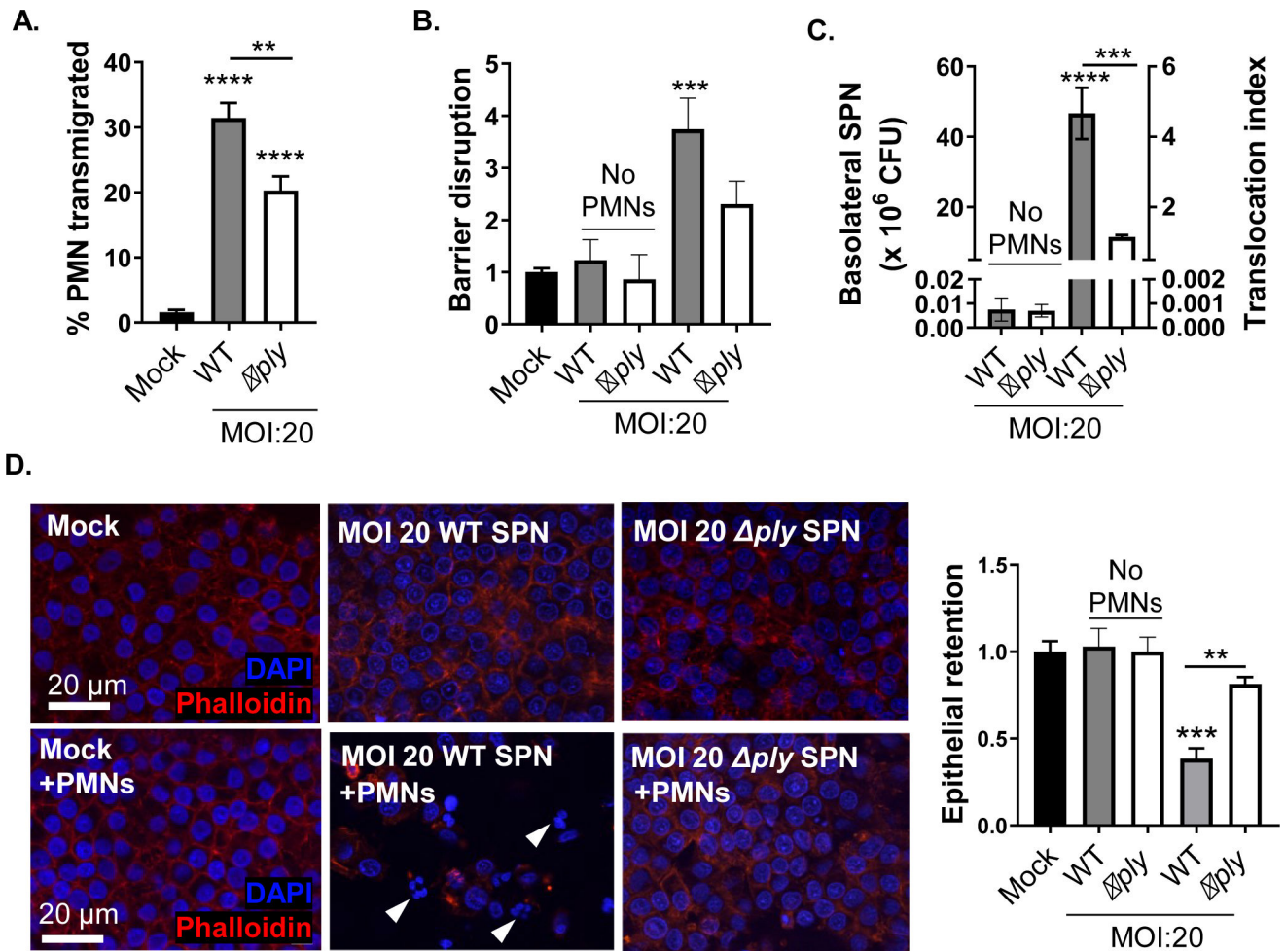
FIG 1 High-dose *S. pneumoniae* infection elicits PLY-dependent PMN recruitment, which promotes epithelial detachment and bacterial translocation. (A) 1 × 10^6 human PMNs were added to the basolateral side of Transwell seeded polarized H292 monolayers that were mock-infected (with HBSS, "Mock"), infected apically with wild-type TIGR4 ("WT"), or infected apically with a pneumolysin-deficient mutant ("*Δply*") at the indicated MOI for 2.5 h. Subsequently, PMN transepithelial migration after 2.5 h was quantified by MPO activity. (B) Barrier integrity of monolayers was measured by HRP flux post-infection, normalized to mock-infected. (C) Transepithelial migration of bacteria was quantitated by plating for CFUs, and the translocation index was determined by normalizing SPN present in the basolateral compartment to the infection inoculum. (D) Fluorescence microscopy of monolayers stained with DAPI (blue) and phalloidin (red). White arrows indicate PMN nuclei. Scale bar = 20 µm. Epithelial cell retention was quantified by epithelial cell nuclei number per field of view. Each panel shown is representative of three independent experiments in triplicates, or pooled data from at least three independent experiments. Error bars represent mean ± SEM. Statistical analysis was performed using ordinary one-way ANOVA: *P-value ≤ 0.05, **P-value ≤ 0.01, ***P-value ≤ 0.001, ****P-value ≤ 0.0001.

significant PI staining, suggesting that PLY permeabilized cells during infection (Fig. S1C). Although we and others have shown that H292 cells initiate membrane repair processes to prevent cell death following PLY insult (20, 44), it is possible that PLY-permeabilized cells are particularly vulnerable to dislocation from the monolayer upon subsequent addition of PMNs. We thus examined monolayer confluency by IF again post PMN transmigration. PMN infiltration to WT TIGR4 infected monolayers can be identified by their multi-lobed nuclei (Fig. 1D, white arrowheads), and PMN migration was associated with loss of 62% of epithelial cells from the monolayer (Fig. 1D, bottom row, "Mock" vs "WT SPN," with image analysis quantitation on right). In contrast, infection by TIGR4*Δply* resulted in a 20% loss of epithelial cells, significantly less than the loss associated with infection by WT TIGR4 ($P < 0.01$) (Fig. 1D).

Because PLY can also permeabilize PMNs, we used flow cytometry to evaluate the degree of PI staining after direct infection of PMN with WT or TIGR4*Δply* and observed a PLY-dependent permeabilization of 2% of PMNs (Fig. S1D). We also evaluated PMN

permeabilization after traversing the monolayer by measuring MPO activity in the apical buffer immediately after PMN transmigration. We observed a two-fold and significant increase in MPO activity in WT TIGR4 infected Transwells (Fig. S1E), which corresponds to if approximately 10% of transmigrated PMNs released MPO. No MPO activity above background was observed with TIGR4Δ*ply* infection. This raises the possibility that at an MOI of 20, PMN release of effector molecules post transmigration may contribute to epithelial detachment. These findings implicate PMN transmigration, augmented by PLY, as a key factor that drives monolayer disruption, barrier integrity compromise, and *S. pneumoniae* translocation.

Low-dose infection elicits PLY-dependent PMN recruitment, which drives *S. pneumoniae* translocation in the absence of epithelial detachment

PMN transmigration in response to TIGR4 infection is highly MOI-dependent (21, 31). Hence, we performed a similar series of experiments infecting H292 monolayers with a 10-fold lower infection dose, which resulted in approximately 1×10^5 total bacteria bound/Transwell (Fig. S1A). WT TIGR4 infection at MOI 2 triggered transmigration of ~15×10^4 human PMNs (i.e., 15% of total PMNs added; Fig. 2A, "WT"), approximately two-fold lower than that observed at an MOI of 20 (Fig. 1A, "WT"), yet 30-fold higher ($P < 0.01$) compared to mock-infected monolayers. Infection with TIGR4Δ*ply* resulted in an approximate six-fold (and not statistically significant) increase in PMN transmigration compared to mock-infected monolayers, indicating that PMN transmigration remains PLY-promoted at the lower MOI (Fig. 2A, "Δ*ply*"). Notably, this PLY-dependent effect was not due to more efficient bacteria-host cell interaction because monolayer binding by TIGR4Δ*ply* was indistinguishable from WT (Fig. S1A), nor due to host cell killing by PLY because epithelial and neutrophil viability was not affected at this MOI (Fig. S1B–E). Disruption of barrier integrity correlated with PMN transmigration, because HRP flux was elevated 2.2-fold ($P < 0.01$) upon infection with WT TIGR4 but not significantly by TIGR4Δ*ply* compared to mock-infected monolayers (Fig. 2B). Correspondingly, at MOI 2, 0.9×10^6 WT TIGR4 and 0.2×10^6 TIGR4Δ*ply* bacteria migrated to the basolateral chamber, respectively (Fig. 2C). While the lower number of bacteria translocated was expected given the lower inoculum, it is notable that translocation was still PMN-promoted because in the absence of PMNs, translocation of WT TIGR4 and TIGR4Δ*ply* was diminished 700- and 300-fold, respectively (Fig. 2C). Monolayer confluency was retained despite robust PMN and *S. pneumoniae* transmigration (Fig. 2D). Hence, at an MOI of 2, PLY and PMNs promoted bacterial migration in a manner that did not require overt destruction of the monolayer.

To determine whether the pro-transmigration functions of PLY were restricted to PLY-producing bacteria or could function in *trans*, we infected H292 monolayers with either a 1:1 or 1:9 mixture of WT TIGR4 and TIGR4Δ*ply*, where TIGR4Δ*ply* can be identified through chloramphenicol resistance. To avoid the epithelial detachment that is associated with the MOI 20 dose (Fig. 1D), we utilized the MOI of 2 dose. As shown previously in Fig. 2A, WT TIGR4 elicited a stronger PMN response than TIGR4Δ*ply* (Fig. 2E). Both the 1:1 and the 1:9 mixed infections led to neutrophil recruitment similar to that of WT TIGR4-infected monolayers (Fig. 2E), consistent with previous reports of PLY-mediated PMN chemoattractant HXA$_3$ secretion by host cells (20). In the presence of transmigrating PMNs, bacteria from both the 1:1 and 1:9 mixed infections efficiently migrated to the basolateral compartment with efficiencies similar to that of infections with WT TIGR4 only (Fig. 2F). Differential antibiotic resistance permitted distinction between the two strains and revealed that the transmigration of TIGR4Δ*ply* was significantly ($P < 0.05$, indicated by "#") increased in the presence of WT TIGR4 (Fig. 2F). Moreover, the ratio of WT:Δ*ply* bacteria in the basolateral chamber was similar to input ratios upon apical infection, that is, the 1:1 WT:Δ*ply* mixture resulted in a 1 : 1.4 output and the 1:9 input resulted in a 1 : 5.7 output (Fig. 2F). Thus, the pro-translocation activity of PLY promotes migration of both PLY-producing and -deficient bacteria, likely by eliciting epithelial cell
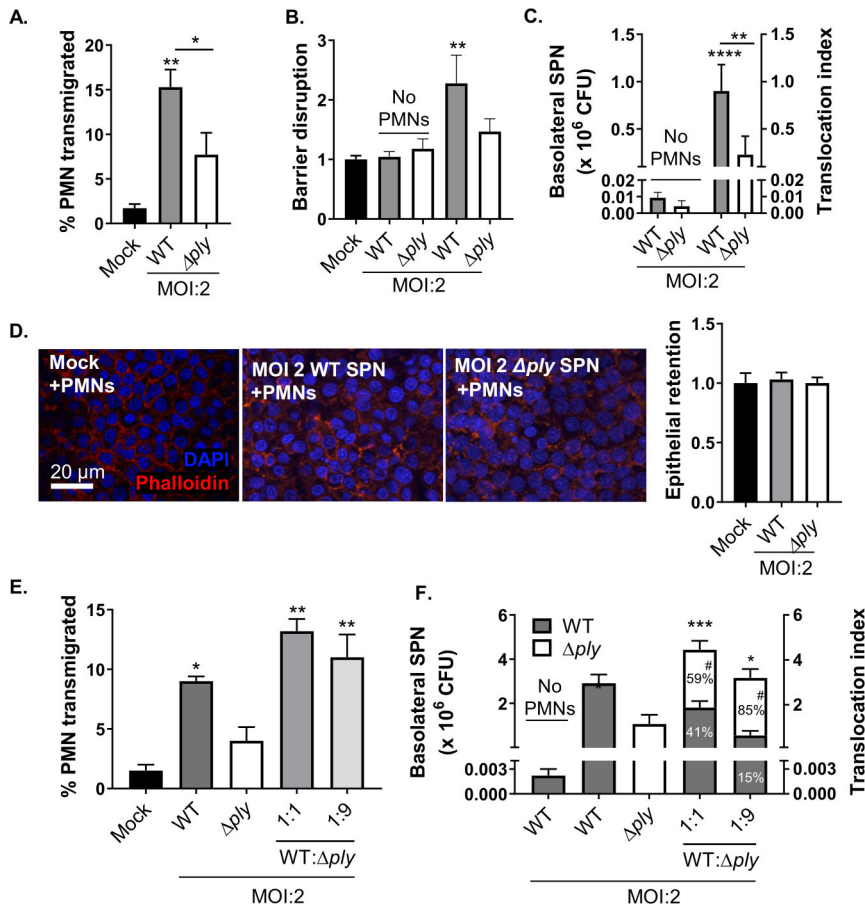
FIG 2 Low-dose infection elicits PLY-dependent PMN recruitment, which drives *S. pneumoniae* translocation in the absence of epithelial detachment. (A) 1×10^6 human PMNs were added to the basolateral side of monolayer mock-infected (with HBSS "Mock") or infected apically with WT or *Δply* SPN at indicated MOI. PMN transepithelial migration was quantified by MPO activity. (B) Barrier integrity of monolayers was measured by HRP flux post-infection, normalized to mock-infected. (C) Transepithelial migration of bacteria was quantitated by plating for CFUs, and translocation index was determined by normalizing SPN present in basolateral chamber to infection inoculum. (D) Fluorescence microscopy of monolayers stained with DAPI (blue) and phalloidin (red). Scale bar = 20 μm. Epithelial cell retention was quantified by epithelial cell nuclei number per field of view. (E) Monolayers were mock-infected (HBSS) or apically infected with WT, *Δply*, a 1:1 mix of WT and *Δply*, or a 1:9 mix of WT and *Δply* SPN at indicated MOI. PMN transepithelial migration was quantified by MPO activity. (F) Transepithelial migration of bacteria was quantitated by plating, and translocation index was determined by normalizing SPN migration to infection inoculum. Statistical analysis comparing total SPN migration between respective groups indicated with "*," statistical analysis comparing TIGR4*Δply* migration between respective groups indicated with "#." Each panel shown is representative of three independent experiments in triplicates, or pooled data from at least three independent experiments. Error bars represent mean ± SEM. Statistical analysis was performed using ordinary one-way ANOVA: *P-value ≤ 0.05, **P-value ≤ 0.01, ***P-value ≤ 0.001.

HXA$_3$ production and concomitant PMN migration, which contributes to barrier disruption (20).

S. pneumoniae infection results in cleavage and mislocalization organization of the AJ protein E-cadherin via PLY-dependent and -independent pathways

S. pneumoniae has been reported to target endothelial and epithelial junctional components to compromise respiratory barrier function (4). To determine if *S.*

pneumoniae targets junctional components in our model, we infected H292 cell monolayers and stained with an antibody that recognizes the extracellular domain of E-cadherin, a transmembrane AJ protein capable of homotypic binding to promote barrier formation that is robustly expressed by H292 cells. When visualized by IF microscopy, E-cadherin is located in circumferential rings at the cell periphery (Fig. 3A, "Mock"; Fig. S2). Addition of PMNs to a mock-infected monolayer had no effect on E-cadherin localization of staining intensity visualized by IF (Fig. 3A, "Mock +PMNs").

To examine whether H292 cell E-cadherin complexes are disrupted upon PMN migration induced by *S. pneumoniae*, monolayers were apically infected with WT TIGR4 or TIGR4Δ*ply* at an MOI of 20 or 2. WT TIGR4 infected monolayers lost all cell periphery E-cadherin, regardless of infection dose (Fig. 3A, top row, "WT SPN"; Fig. S2). In contrast, TIGR4Δ*ply* was able to induce loss pericellular E-cadherin localization at an MOI of 20 but not at an MOI of 2 (Fig. 3A, bottom row, "Δ*ply* SPN"). Quantification of E-cadherin localization specifically at the cell periphery was carried out with the IJOQ script (43), which quantifies the continuity in pericellular staining. This analysis showed both WT TIGR4 and TIGR4Δ*ply* infection at an MOI of 20 eliminated E-cadherin organization ($P <$ 0.0001), whereas at an MOI of 2, only WT TIGR4 infection induced a significant (60%) reduction in E-cadherin organization ($P < 0.0001$) (Fig. 3B).

To determine if E-cadherin structure is altered by infection by *S. pneumoniae*, we performed western blotting of E-cadherin in total cell lysates from uninfected or infected monolayers. This revealed a PLY-dependent decrease in the 130 kDa full-length E-cadherin and the appearance of an E-cadherin-related 30 kDa species after infection with WT TIGR4 at MOI 20 (Fig. 3C). At MOI 2, infection by WT TIGR4 also resulted in apparent E-cadherin cleavage, although densitometric analysis did not reveal statistical significance (Fig. 3D). E-cadherin cleavage appeared to be partially dependent on PLY, because infection by TIGR4 Δ*ply* at either MOI 2 or 20 resulted in less cleavage than during WT infection (Fig. 3C and D, "Δ*ply*"). Thus, E-cadherin cleavage and mislocalization is triggered via both PLY-dependent and -independent pathways, with the PLY-dependent pathway capable of triggering these changes at a lower infectious dose.

PMNs are not required for E-cadherin mislocalization by *S. pneumoniae* at either low or high infectious dose

Independent of PMNs, *S. pneumoniae* has been reported to downregulate epithelial junctional components during infection through mechanisms such as TLR2 engagement (9) and pneumococcal neuraminidase activity (15). To determine whether PMNs are required for the PLY-dependent and -independent E-cadherin mislocalization described earlier, we infected monolayers with WT TIGR4 and TIGR4Δ*ply* at an MOI of 20 or 2 in the absence of PMNs. At an MOI of 20, both WT TIGR4 and TIGR4Δ*ply* depleted all pericellular E-cadherin (Fig. 4A), just as when PMNs were present (Fig. 3A). Lowering the MOI to 2, we observed that WT TIGR4 induced a 38% ($P < 0.01$) decrease in E-cadherin localization to cell periphery (Fig. 4B, top row, "MOI 2 WT SPN," and right, solid bars). In contrast, TIGR4Δ*ply* infection at an MOI of 2 had no effect on E-cadherin localization (Fig. 4B, top row, "MOI 2 Δ*ply* SPN," and right, solid bars).

To determine if *S. pneumoniae* disruption of E-cadherin integrity could be augmented by the addition of purified PLY, we added recombinant PLY at a sublytic PLY concentration of 0.01 toxin activity units (see Materials and Methods) (20), a concentration that by itself was incapable of disrupting E-cadherin localization (Fig. 4B, "Mock, 0.01U PLY," and right, open bars). We found that, when combined with infection by WT TIGR4, this level of exogenous PLY enhanced E-cadherin disruption from 38% to 81% ($P < 0.01$; Fig. 4B, bottom row, "WT SPN, 0.01U PLY," and right, open bars). Whereas TIGR4Δ*ply* at an MOI of 2 was insufficient to perturb E-cadherin on its own, the addition of 0.01U PLY to monolayers infected with TIGR4Δ*ply* resulted in a 53% ($P < 0.001$) reduction in E-cadherin cell periphery organization (Fig. 4B, "Mock +0.01U PLY," and right, open bar).
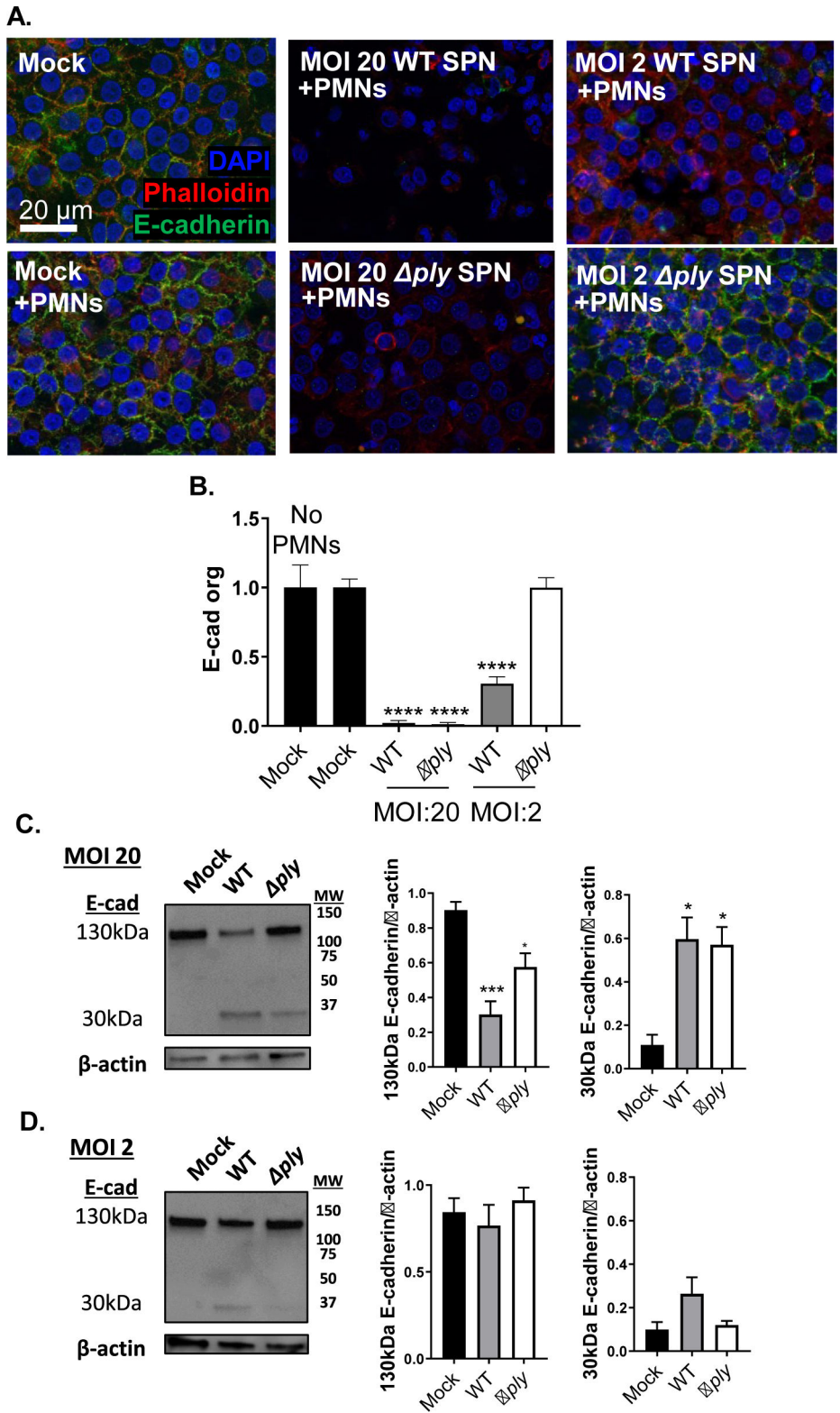
FIG 3 *S. pneumoniae* cleaves and disrupts the localization of E-cadherin via PLY-dependent and -independent pathways. (A) 1 × 10^6 human PMNs were added to the basolateral side of monolayers mock-infected (HBSS) or infected apically with WT or *Δply* SPN at indicated MOI. Monolayers were stained with ectodomain E-cadherin antibody (green) before permeabilization and with DAPI (blue) and phalloidin (red) after permeabilization. Scale bar = 20 µm. (B) Peripheral E-cadherin organization was (Continued on next page)

Because PLY promotes PMN transmigration (18, 20), we hypothesized that the addition of PMNs to monolayers infected with WT TIGR4 may further compromise E-cadherin integrity. Indeed, the addition of PMNs to the basolateral chamber of monolayers infected with WT TIGR4 at an MOI of 2 resulted in a two-fold decrease ($P < 0.05$) in E-cadherin organization (Fig. 4C, "WT" vs "WT + PMN"). As expected, PLY was critical to this augmentation, because the addition of PMNs to monolayers infected with TIGR4Δply had no effect (Fig. 4C, "Δply" vs "Δply + PMN").

Pore formation by PLY and related toxins is necessary and sufficient for E-cadherin mislocalization

To investigate whether purified PLY is sufficient for disrupting E-cadherin localization, we examined E-cadherin organization after apical treatment of H292 monolayers with various concentrations of PLY. 1U of PLY, a concentration resulting in transient permeabilization of 50% of host cell followed by membrane repair (20), ablated pericellular E-cadherin (Fig. 5A). A 10-fold lower PLY concentration also significantly ($P < 0.05$) reduced E-cadherin organization compared to mock treatment (Fig. 5A). 0.01U of PLY had no effect on E-cadherin organization (Fig. 5A). Thus, purified PLY mimics E-cadherin disruption by live *S. pneumoniae*, and in an infection dose-dependent manner. Western blotting of E-cadherin confirmed no cleavage of E-cadherin with 0.01U PLY treatment, partial diminution of full-length E-cadherin and the appearance of a very faint 30 kDa species with 0.1U PLY treatment, and a dramatic reduction in full-length E-cadherin and the appearance of the 30 kDa cleavage product with 1U PLY treatment (Fig. 5B).

MMPs, which can be released by epithelial cells or PMNs during infection, are capable of cleaving extracellular matrix and junctional proteins, including E-cadherin (27, 45, 46). The pore-forming *Staphylococcus aureus* α-toxin (47, 48) and *Pseudomonas aeruginosa* exolysin (49) trigger E-cadherin cleavage in infected cells by activating host MMPs. PLY also has been shown to trigger MMP activation in A549 cells (47). We found that treatment of either epithelial cells or PMNs with 1U of purified PLY triggered an increase of MMP activity in cell supernatants (Fig. S3A and B). This activity was inhibited by the broad-spectrum MMP inhibitor GM6001. However, the MMP inhibitor GM6001 did not prevent E-cadherin cleavage (Fig. 3C, "GM6001") or disruption of E-cadherin organization when monolayers were treated with 1U PLY or infected with WT TIGR4 at MOI 2 (Fig. S3C and D), implying that E-cadherin disuption observed was not mediated by MMPs.

Many of the biologic activities of PLY are mediated through its pore-forming activity (35), but PLY is also capable of altering cell behavior independent of pore-formation (34, 36). The mutant PLY$^{T459G \cdot L460G}$ (which we herein term "PLY$_{CBS}$") is mutated at two critical residues in the cholesterol binding site in PLY domain 4 and incapable of pore-formation (20, 50). H292 monolayers treated with PLY$_{CBS}$ at equimolar concentration to 1U PLY had no effect on E-cadherin integrity by microscopy (Fig. 5C and D). Likewise, apical infection with TIGR4 mutant producing PLY$_{CBS}$ (PLY$_{CBS}$ SPN), which is incapable of H292 cell permeabilization, failed to disrupt H292 E-cadherin organization (Fig. 5E and F), indicating that pore-formation by PLY is essential for E-cadherin disruption.

PLY belongs to a family of CDCs that share substantial structural and functional conservation. We investigated whether other CDCs could also induce E-cadherin disruption. H292 monolayers apically treated with 1U of perfringolysin O (PFO) or intermedilysin (ILY) resulted in almost complete ablation of E-cadherin staining (Fig. 5G and H), like that observed with 1U of PLY. These results indicate that the ability to disrupt pericellular localization of the epithelial cell AJ protein E-cadherin is a property conserved among CDCs and may be utilized by many CDC-expressing bacterial pathogens to target host cell junction networks.
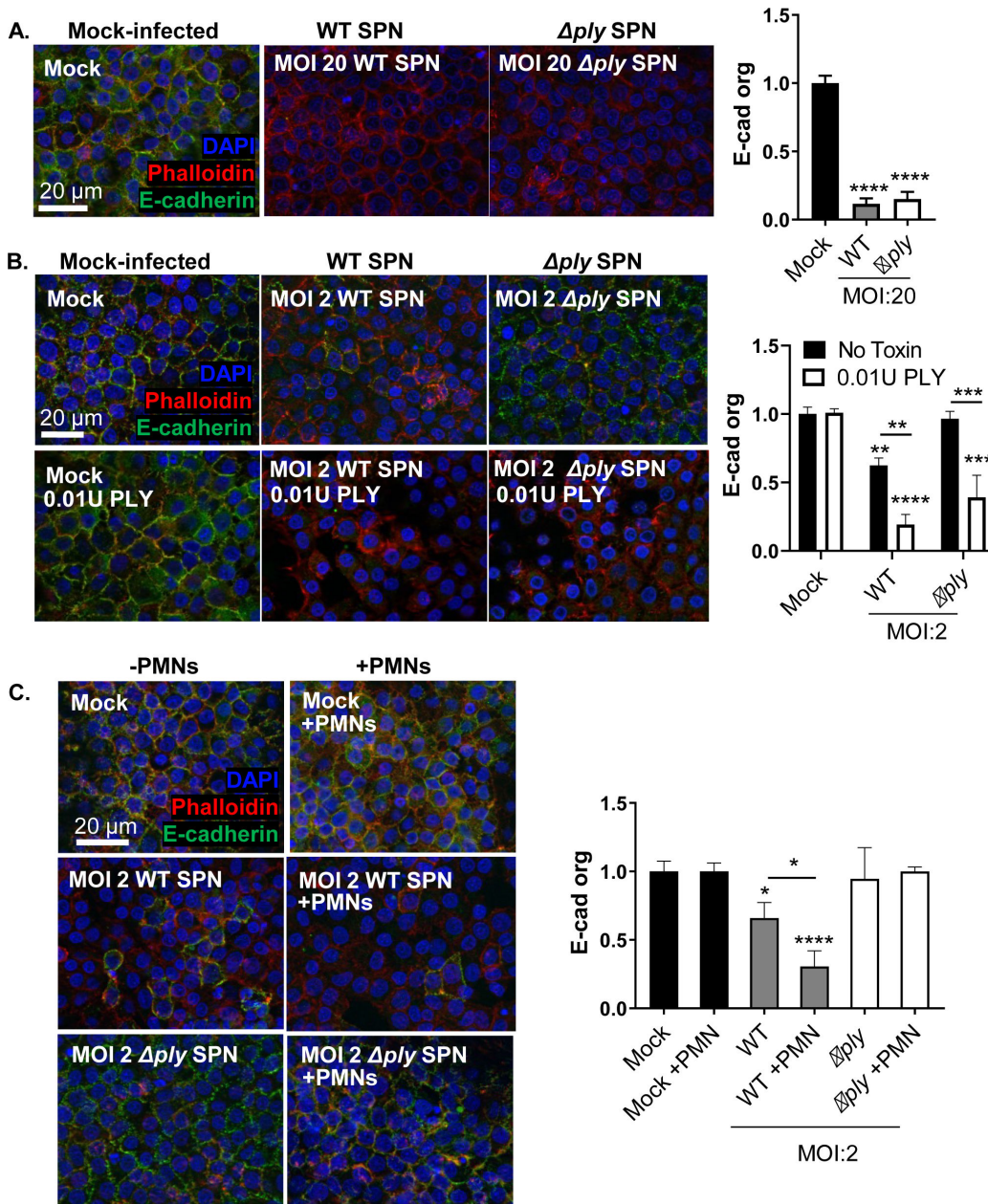
FIG 4 PMNs are not required for E-cadherin mislocalization by *S. pneumoniae* at either low or high infectious dose (A) Fluorescence microscopy of monolayers mock-infected (HBSS) or infected apically with WT or *Δply* SPN at indicated MOI in the absence of PMNs, stained with ectodomain E-cadherin antibody (green) before permeabilization and with DAPI (blue) and phalloidin (red) after permeabilization. Scale bar = 20 μm. Peripheral E-cadherin organization was quantitated by image analysis with IJOQ. (B) Fluorescence microscopy of monolayers mock-infected (HBSS) or infected apically with WT or *Δply* SPN at indicated MOI, and complemented with recombinant PLY where indicated. Monolayers were stained with ectodomain E-cadherin antibody (green) before permeabilization and with DAPI (blue) and phalloidin (red) after permeabilization. Scale bar = 20 μm. Peripheral E-cadherin organization was quantitated by image analysis with IJOQ. (C) Fluorescence microscopy of monolayers mock-infected with HBSS (mock) or infected apically with WT or *Δply* SPN at indicated MOI in the presence or absence of PMNs, stained with ectodomain E-cadherin antibody (green) before permeabilization and with DAPI (blue) and phalloidin (red) after permeabilization. Scale bar = 20 μm. Peripheral E-cadherin organization was quantitated by image analysis with IJOQ. Each panel shown is representative of three independent experiments in triplicates. Error bars represent mean ± SEM. Statistical analysis was performed using ordinary one-way ANOVA: *P-value ≤ 0.05, **P-value ≤ 0.01, ***P-value ≤ 0.001.
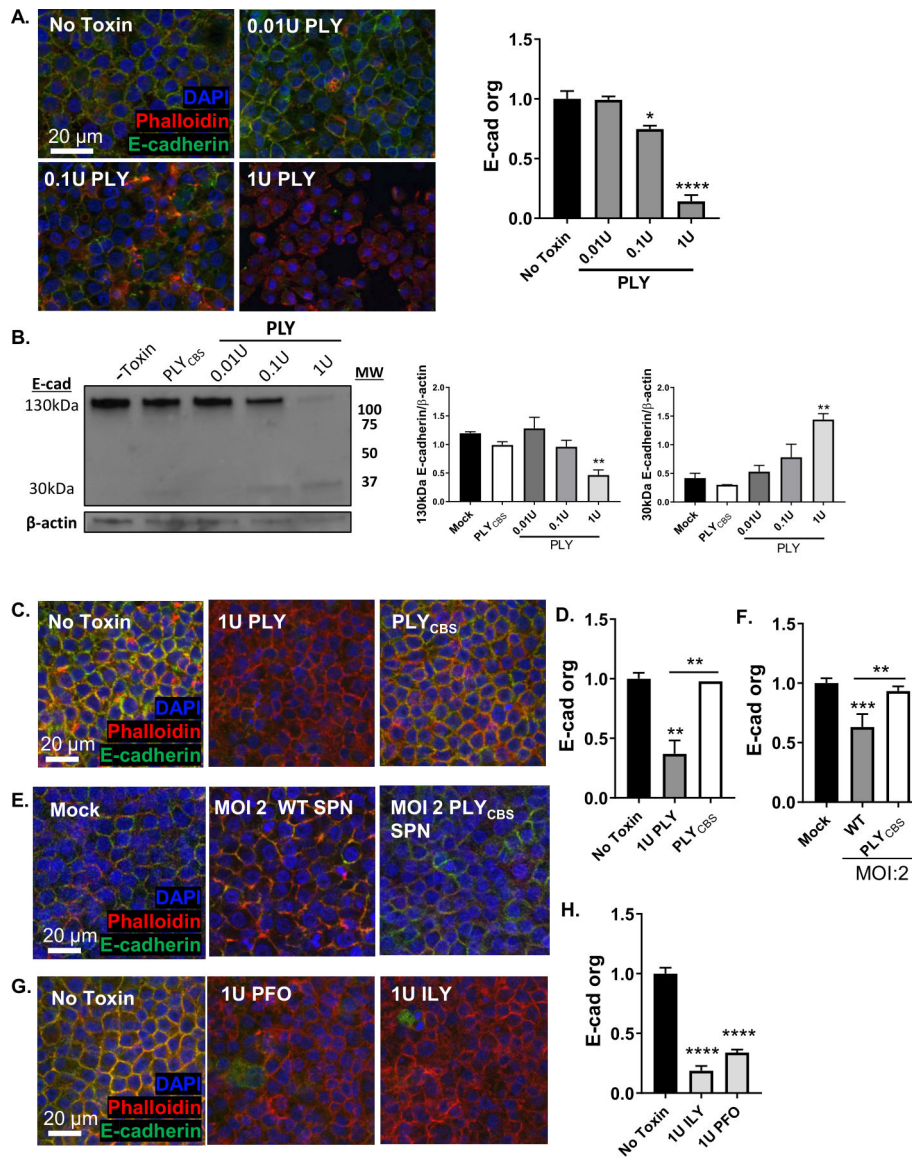
FIG 5 Treatment of epithelial cells by PLY or related pore-forming toxins is sufficient to induce cleavage and mislocalization of E-cadherin. Monolayers were treated with HBSS (no toxin) or the indicated units of recombinant PLY. (A) Monolayers were stained with ectodomain E-cadherin antibody (green) before permeabilization and with DAPI (blue) and phalloidin (red) after permeabilization. Scale bar = 20 µm. Peripheral E-cadherin organization was quantitated by image analysis with IJOQ. (B) Monolayers were lysed for western blotting of E-cadherin and desitometry analysis normalized to β-actin. (C) Fluorescence microscopy of monolayers treated apically with purified PLY$_{CBS}$ protein at equimolar concentrations to 1U of PLY. Monolayers were permeabilized and stained with E-cadherin antibody (green), DAPI (blue), and phalloidin (red). Scale bar = 20 µm. (D) Peripheral E-cadherin organization was quantitated by image analysis with IJOQ. (E) Fluorescence microscopy of monolayers infected apically with PLY$_{CBS}$-expressing SPN (PLY$_{CBS}$ SPN) at indicated MOI. Monolayers were permeabilized and stained with E-cadherin antibody (green), DAPI (blue), and phalloidin (red). Scale bar = 20 µm. (F) Peripheral E-cadherin organization was quantitated by image analysis with IJOQ. (G) Fluorescence microscopy of monolayers treated with the indicated units of purified PLY, intermedilysin (ILY) of *S. intermedius*, or perfringolysin O (PFO) of *C. perfringens*. Monolayers were permeabilized and stained with E-cadherin antibody (green), DAPI (blue), and phalloidin (red). Scale bar = 20 µm. (H) Peripheral E-cadherin organization was quantitated by image analysis with IJOQ. Each panel shown is representative of three independent experiments in triplicates. Error bars represent mean ± SEM. Statistical analysis performed using ordinary one-way ANOVA: *P-value ≤ 0.05, **P-value ≤ 0.01, ***P-value ≤ 0.001, ****P-value ≤ 0.0001.

DISCUSSION

The mucosal epithelium, sealed by a well-organized system of intercellular junctional complexes, is a physical line of defense against microbial invasion. Pathogens that cross epithelial barriers often disrupt these epithelial junctions, which facilitates tissue invasion by paracellular movement (51). *S. pneumoniae* has been shown to target airway junction proteins and compromise airway epithelial barrier function (4, 9, 10). Pneumococcal infection reduces alveolar occludin, ZO-1, claudin-5, and VE-cadherin in human lung explants (4), and downregulates claudin-7 and −10 in murine models (9). The reduction in critical junctional molecules can increase epithelial permeability and is likely an important step in facilitating pneumococcal dissemination (52); mice deficient in type I interferon, which show junctional defects in response to bacterial infection, are highly susceptible to *S. pneumoniae* bacteremia (10). We thus examined the epithelial barrier and junctional integrity during *S. pneumoniae* infection of polarized H292 monolayers to systematically reveal requirements for *S. pneumoniae* translocation across the respiratory epithelium. We show that PLY and transmigrating PMNs (1) individually and cooperatively perturb localization and integrity of the AJ protein E-cadherin, (2) cause distinct degrees of epithelial damage depending on infection dose, PLY-mediated pore formation, and PMN presence, and (3) only when combined promote maximal bacterial cross-epithelial dissemination.

PLY, a *S. pneumoniae* virulence factor present in almost all clinical isolates of the species, increases alveolar permeability and alveolar epithelial cell injury (53). In human adenoid epithelial explant cultures, PLY ablates TJs and exposes host receptors for bacterial attachment (13). The notable invasiveness of serotype 1 pneumococci has been attributed to its rapid and robust release of PLY, which promotes ZO-1 disruption (14). Here, we found that *S. pneumoniae* at an MOI of 2 triggers both cleavage and mislocalization of the junctional protein E-cadherin in a manner dependent on PLY-mediated pore-forming activity. Two other CDCs, ILY and PFO, induce intercellular junction disruption, suggesting that junction disruption is a conserved function of CDCs (54, 55). Other pathogens, such as *Staphylococcus aureus, Pseudomonas aeruginosa,* and *Serratia marcescens,* produce non-CDC pore-forming toxins that disrupt junctions *in vitro* (47, 49).

The ability of *S. pneumoniae* at an MOI (of 2) that did not compromise host cell membrane integrity indicates that E-cadherin disorganization is not a simple consequence of host cell death (20). PLY, like other pore-forming toxins, triggers membrane repair (44, 56–58), and, by activating GTPases that regulate actin assembly (11), may destabilize actin-associated junctional protein complexes (59, 60). PLY, although not a protease itself, has been shown to increase metalloprotease activity in A549 cells (47). Pore-forming toxins of *P. aeruginosa* and *S. marcescens* induce an influx of calcium ions, thus activating the calmodulin-regulated metalloproteinase ADAM-10, which cleaves E-cadherin (61). *S. aureus* toxin Hla directly binds and activates ADAM-10. Western blotting revealed a 30 kDa cleavage product was generated upon *S. pneumoniae* infection or PLY treatment, suggesting disruption of E-cadherin organization is associated with its proteolytic cleavage. Consistent with previous reports (47, 48), we found that infection of PMNs or epithelial cells by PLY-producing SPN or treatment with purified PLY was associated with an increase in MMP activity in culture supernatants. However, inhibition of MMP did not prevent E-cadherin cleavage or mislocalization. Identification of proteases responsible for PLY-dependent cleavage of E-cadherin organization warrants future studies.

At an MOI of 20, both PLY-producing and -deficient *S. pneumoniae* disrupted junctional organization of H292 cell monolayers. This PLY-independent pathway augments PLY-mediated disruption, as a PLY concentration (0.01U) that was insufficient for E-cadherin loss in isolation, in combination with PLY-deficient *S. pneumoniae* facilitated complete junctional disruption. TLR stimulants (9) and pneumococcal neuraminidase (15), which downregulate junctional components, are potential non-PLY bacterial factors that contribute to E-cadherin loss.

S. pneumoniae-mediated junctional disruption of monolayers alone was insufficient to promote bacterial translocation. Neutrophils secrete proteolytic enzymes capable of cleaving extracellular matrix and junctional proteins (27, 28, 62, 63), and PMN transmigration triggered by HXA$_3$ was required for barrier breach of pulmonary epithelium by *S. pneumoniae* (21, 31). PLY, which triggers epithelial production of HXA$_3$ (20), may enhance bacterial translocation. Indeed, a highly invasive *S. pneumoniae* serotype 1 strain, which releases high levels of PLY, induces severe inflammation of the lung, with ~4-fold more neutrophils than a serotype 2 strain tested in parallel (14).

Although PLY clearly promotes PMN transmigration, monolayer infection with TIGR4Δ*ply* also triggered (lower levels of) neutrophil movement, presumably due to the production of chemoattractants in response to (non-PLY) bacterial products (64, 65). The level of barrier breach by TIGR4Δ*ply* in the presence of PMNs appeared elevated compared to background levels (Figures 1 and 2) but these higher levels did not reach statistical significance. Interestingly, at an MOI of 20, PMN transmigration in response to *S. pneumoniae* infection resulted in the PLY-dependent loss of more than 50% of the epithelial monolayer, a loss that correlated with the efficient transepithelial movement of the marker HRP and the apparently unimpeded barrier breach by pneumococci. Epithelial detachment by activated neutrophils has been observed for several cell lines (66, 67) and has been correlated with secreted neutrophil elastase, which, during pneumococcal pneumonia, causes extensive tissue damage in both mouse models and humans (68, 69). Although dramatic epithelial loss provides an explanation for PLY- and PMN-promoted bacterial transmigration at an MOI of 20, at a lower MOI, WT TIGR4 was capable of barrier breach in the absence of monolayer destruction, indicating that frank epithelial loss is not required for PLY-promoted bacterial movement in this experimental system.

In summary, by manipulating infectious dose and the presence or absence of PLY or PMNs during apical infection of polarized epithelial monolayers by *S. pneumoniae* alters the epithelium and its interaction with PMNs in multiple ways. The bacterium utilizes PLY-dependent and -independent mechanisms to induce cleavage and mislocalization of E-cadherin, as well as to recruit PMNs across respiratory epithelial cell monolayers. Notably, E-cadherin disruption alone was insufficient to induce significant bacterial movement across epithelium, which instead depended on PMN transmigration. These studies provide further insight into the multifaceted role of PLY in pulmonary inflammation and barrier breach during *S. pneumoniae* lung infection.

AUTHOR AFFILIATIONS

[1]Department of Molecular Biology and Microbiology, Tufts University, Boston, Massachusetts, USA

[2]Program in Immunology, Tufts Graduate School of Biomedical Sciences, Boston, Massachusetts, USA

[3]Department of Biological Sciences, San Jose State University, San Jose, California, USA

[4]Department of Microbiology and Environmental Toxicology, University of California, Santa Cruz, California, USA

[5]University of Puerto Rico, Cayey, USA

[6]Francisco de Vitoria University, Madrid, Spain

[7]Department of Microbiology and Immunology, University of Oklahoma Health Sciences Center, Oklahoma, Oklahoma, USA

[8]Stuart B. Levy Center for Integrated Management of Antimicrobial Resistance at Tufts (Levy CIMAR), Boston, Massachusetts, USA

AUTHOR ORCIDs

Shuying Xu http://orcid.org/0000-0003-4572-8663
Walter Adams http://orcid.org/0000-0002-2979-1382

FUNDING

AUTHOR CONTRIBUTIONS

ETHICS APPROVAL

All work with human donors was approved by the Tufts University Human Investigation Review Board (IRB). Written informed consent was obtained from all donors and collection was carried out with the assistance of services provided by the Tufts Clinical and Translational Research Center (CTRC).

ADDITIONAL FILES

The following material is available online.

Supplemental Material

Fig. S1 (IAI00213-23_s0001.tif). PLY-producing *S. pneumoniae* induces membrane permeabilization of epithelial cells and PMNs at high- but not low-dose infection.
Supplemental figure legends (IAI00213-23_s0004.docx). Legends for supplemental Figures S1 to S3.
Fig. S2 (IAI00213-23_s0002.tif). Single-channel IF microscopy images of polarized H292 monolayers infected with the indicated MOI of WT *S. pneumoniae*.
Fig. S3 (IAI00213-23_s0003.tif). PLY enhances MMP activity in culture supernatants of both epithelial cells and PMNs but MMP inhibition does not protect against junctional damage.

REFERENCES

1. CDC. 2019. Pneumococcal disease. Available from: https://www.cdc.gov/pneumococcal/index.html. Retrieved 18 May 2019.
2. Chen H, Matsumoto H, Horita N, Hara Y, Kobayashi N, Kaneko T. 2021. Prognostic factors for mortality in invasive Pneumococcal disease in adult: a system review and meta-analysis. Sci Rep 11:11865. https://doi.org/10.1038/s41598-021-91234-y
3. Ganesan S, Comstock AT, Sajjan US. 2013. Barrier function of airway tract epithelium. Tissue Barriers 1:e24997. https://doi.org/10.4161/tisb.24997
4. Peter A, Fatykhova D, Kershaw O, Gruber AD, Rueckert J, Neudecker J, Toennies M, Bauer TT, Schneider P, Schimek M, Eggeling S, Suttorp N, Hocke AC, Hippenstiel S. 2017. Localization and pneumococcal alteration of junction proteins in the human alveolar-capillary

compartment. Histochem Cell Biol 147:707–719. https://doi.org/10.1007/s00418-017-1551-y

5. Otani T, Furuse M. 2020. Tight junction structure and function revisited. Trends Cell Biol 30:805–817. https://doi.org/10.1016/j.tcb.2020.08.004

6. Bhatt T, Rizvi A, Batta SPR, Kataria S, Jamora C. 2013. Signaling and mechanical roles of E-cadherin. Cell Commun Adhes 20:189–199. https://doi.org/10.3109/15419061.2013.854778

7. Georas SN, Rezaee F. 2014. Epithelial barrier function: at the front line of asthma Immunology and allergic airway inflammation. J Allergy Clin Immunol 134:509–520. https://doi.org/10.1016/j.jaci.2014.05.049

8. Wittekindt OH. 2017. Tight Junctions in pulmonary epithelia during lung inflammation. Pflugers Arch 469:135–147. https://doi.org/10.1007/s00424-016-1917-3

9. Clarke TB, Francella N, Huegel A, Weiser JN. 2011. Invasive bacterial pathogens exploit TLR-mediated downregulation of tight junction components to facilitate translocation across the epithelium. Cell Host Microbe 9:404–414. https://doi.org/10.1016/j.chom.2011.04.012

10. LeMessurier KS, Häcker H, Chi L, Tuomanen E, Redecke V. 2013. Type I interferon protects against pneumococcal invasive disease by inhibiting bacterial transmigration across the lung. PLoS Pathog 9:e1003727. https://doi.org/10.1371/journal.ppat.1003727

11. Iliev AI, Djannatian JR, Nau R, Mitchell TJ, Wouters FS. 2007. Cholesterol-dependent actin remodeling via RhoA and Rac1 activation by the Streptococcus pneumoniae toxin pneumolysin. Proc Natl Acad Sci U S A 104:2897–2902. https://doi.org/10.1073/pnas.0608213104

12. Bouillot S, Reboud E, Huber P. 2018. Functional consequences of calcium influx promoted by bacterial pore-forming toxins. Toxins (Basel) 10:387. https://doi.org/10.3390/toxins10100387

13. Rayner CF, Jackson AD, Rutman A, Dewar A, Mitchell TJ, Andrew PW, Cole PJ, Wilson R. 1995. Interaction of pneumolysin-sufficient and -deficient isogenic variants of Streptococcus pneumoniae with human respiratory mucosa. Infect Immun 63:442–447. https://doi.org/10.1128/iai.63.2.442-447.1995

14. Jacques LC, Panagiotou S, Baltazar M, Senghore M, Khandaker S, Xu R, Bricio-Moreno L, Yang M, Dowson CG, Everett DB, Neill DR, Kadioglu A. 2020. Increased pathogenicity of pneumococcal serotype 1 is driven by rapid autolysis and release of pneumolysin. Nat Commun 11:1892. https://doi.org/10.1038/s41467-020-15751-6

15. Gratz N, Loh LN, Mann B, Gao G, Carter R, Rosch J, Tuomanen EI. 2017. Pneumococcal neuraminidase activates TGF-beta signalling. Microbiology (Reading) 163:1198–1207. https://doi.org/10.1099/mic.0.000511

16. Henriques-Normark B, Tuomanen EI. 2013. The pneumococcus: epidemiology, microbiology, and pathogenesis. Cold Spring Harb Perspect Med 3:a010215. https://doi.org/10.1101/cshperspect.a010215

17. Kadioglu A, De Filippo K, Bangert M, Fernandes VE, Richards L, Jones K, Andrew PW, Hogg N. 2011. The integrins mac-1 and alpha$_4$beta$_1$ perform crucial roles in neutrophil and T cell recruitment to lungs during Streptococcus pneumoniae infection. J Immunol 186:5907–5915. https://doi.org/10.4049/jimmunol.1001533

18. Moreland JG, Bailey G. 2006. Neutrophil transendothelial migration in vitro to Streptococcus pneumoniae is pneumolysin dependent. Am J Physiol Lung Cell Mol Physiol 290:L833–40. https://doi.org/10.1152/ajplung.00333.2005

19. Cockeran R, Durandt C, Feldman C, Mitchell TJ, Anderson R. 2002. Pneumolysin activates the synthesis and release of Interleukin-8 by human neutrophils in vitro. J Infect Dis 186:562–565. https://doi.org/10.1086/341563

20. Adams W, Bhowmick R, Bou Ghanem EN, Wade K, Shchepetov M, Weiser JN, McCormick BA, Tweten RK, Leong JM. 2020. Pneumolysin induces 12-lipoxygenase-dependent neutrophil migration during Streptococcus pneumoniae infection. J Immunol 204:101–111. https://doi.org/10.4049/jimmunol.1800748

21. Bhowmick R, Maung N, Hurley BP, Ghanem EB, Gronert K, McCormick BA, Leong JM. 2013. Systemic disease during Streptococcus pneumoniae acute lung infection requires 12-lipoxygenase-dependent inflammation. J Immunol 191:5115–5123. https://doi.org/10.4049/jimmunol.1300522

22. Bou Ghanem EN, Clark S, Roggensack SE, McIver SR, Alcaide P, Haydon PG, Leong JM, Mitchell TJ. 2015. Extracellular adenosine protects against Streptococcus pneumoniae lung infection by regulating pulmonary neutrophil recruitment. PLoS Pathog 11:e1005126. https://doi.org/10.1371/journal.ppat.1005126

23. Lewis ML, Surewaard BGJ. 2018. Neutrophil evasion strategies by Streptococcus pneumoniae and Staphylococcus aureus. Cell Tissue Res 371:489–503. https://doi.org/10.1007/s00441-017-2737-2

24. Beiter K, Wartha F, Albiger B, Normark S, Zychlinsky A, Henriques-Normark B. 2006. An endonuclease allows Streptococcus pneumoniae to escape from neutrophil extracellular traps. Curr Biol 16:401–407. https://doi.org/10.1016/j.cub.2006.01.056

25. Wartha F, Beiter K, Albiger B, Fernebro J, Zychlinsky A, Normark S, Henriques-Normark B. 2007. Capsule and D-alanylated lipoteichoic acids protect Streptococcus pneumoniae against neutrophil extracellular traps. Cell Microbiol 9:1162–1171. https://doi.org/10.1111/j.1462-5822.2006.00857.x

26. Kao SS, Ramezanpour M, Bassiouni A, Wormald PJ, Psaltis AJ, Vreugde S. 2019. The effect of neutrophil serine proteases on human nasal epithelial cell barrier function. Int Forum Allergy Rhinol 9:1220–1226. https://doi.org/10.1002/alr.22401

27. Boxio R, Wartelle J, Nawrocki-Raby B, Lagrange B, Malleret L, Hirche T, Taggart C, Pacheco Y, Devouassoux G, Bentaher A. 2016. Neutrophil elastase cleaves epithelial cadherin in acutely injured lung epithelium. Respir Res 17:129. https://doi.org/10.1186/s12931-016-0449-x

28. Rao RK, Basuroy S, Rao VU, Karnaky KJ, Gupta A. 2002. Tyrosine phosphorylation and dissociation of occludin-ZO-1 and E-cadherin-beta-catenin complexes from the cytoskeleton by oxidative stress. Biochem J 368:471–481. https://doi.org/10.1042/BJ20011804

29. Lax S, Wilson MR, Takata M, Thickett DR. 2014. Using a non-invasive assessment of lung injury in a murine model of acute lung injury. BMJ Open Respir Res 1:e000014. https://doi.org/10.1136/bmjresp-2013-000014

30. José RJ, Williams AE, Mercer PF, Sulikowski MG, Brown JS, Chambers RC. 2015. Regulation of neutrophilic inflammation by proteinase-activated receptor 1 during bacterial pulmonary infection. J Immunol 194:6024–6034. https://doi.org/10.4049/jimmunol.1500124

31. Bhowmick R, Clark S, Bonventre JV, Leong JM, McCormick BA. 2017. Cytosolic phospholipase A2alpha promotes pulmonary inflammation and systemic disease during Streptococcus pneumoniae infection. Infect Immun 85:e00280-17. https://doi.org/10.1128/IAI.00280-17

32. Canvin JR, Marvin AP, Sivakumaran M, Paton JC, Boulnois GJ, Andrew PW, Mitchell TJ. 1995. The role of pneumolysin and autolysin in the pathology of pneumonia and septicemia in mice infected with a type 2 pneumococcus. J Infect Dis 172:119–123. https://doi.org/10.1093/infdis/172.1.119

33. Benton KA, Paton JC, Briles DE. 1997. The hemolytic and complement-activating properties of pneumolysin do not contribute individually to virulence in a pneumococcal bacteremia model. Microb Pathog 23:201–209. https://doi.org/10.1006/mpat.1997.0150

34. Panagiotou S, Chaguza C, Yahya R, Audshasai T, Baltazar M, Ressel L, Khandaker S, Alsahag M, Mitchell TJ, Prudhomme M, Kadioglu A, Yang M. 2020. Hypervirulent pneumococcal serotype 1 harbours two pneumolysin variants with differential haemolytic activity. Sci Rep 10:17313. https://doi.org/10.1038/s41598-020-73454-w

35. Nishimoto AT, Rosch JW, Tuomanen EI. 2020. Pneumolysin: pathogenesis and therapeutic target. Front Microbiol 11:1543. https://doi.org/10.3389/fmicb.2020.01543

36. Subramanian K, Neill DR, Malak HA, Spelmink L, Khandaker S, Dalla Libera Marchiori G, Dearing E, Kirby A, Yang M, Achour A, Nilvebrant J, Nygren P-Å, Plant L, Kadioglu A, Henriques-Normark B. 2019. Pneumolysin binds to the mannose receptor C type 1 (MRC-1) leading to anti-inflammatory responses and enhanced pneumococcal survival. Nat Microbiol 4:62–70. https://doi.org/10.1038/s41564-018-0280-x

37. Neill DRM, Timothy J, Kadioglu A. 2015. Streptococcus pneumoniae: molecular mechanisms of host-pathogen interactions. Academic Press, Amsterdam.

38. Rubins JB, Charboneau D, Paton JC, Mitchell TJ, Andrew PW, Janoff EN. 1995. Dual function of pneumolysin in the early pathogenesis of murine pneumococcal pneumonia. J Clin Invest 95:142–150. https://doi.org/10.1172/JCI117631

39. Kusek ME, Pazos MA, Pirzai W, Hurley BP. 2014. In vitro coculture assay to assess pathogen induced neutrophil Trans-epithelial migration. J Vis Exp 95:142–150. https://doi.org/10.3791/50823

40. Hurley BP, Siccardi D, Mrsny RJ, McCormick BA. 2004. Polymorphonuclear cell transmigration induced by Pseudomonas aeruginosa requires the

eicosanoid hepoxilin A3. J Immunol 173:5712–5720. https://doi.org/10.4049/jimmunol.173.9.5712

41. Shepard LA, Heuck AP, Hamman BD, Rossjohn J, Parker MW, Ryan KR, Johnson AE, Tweten RK. 1998. Identification of a membrane-spanning domain of the thiol-activated pore-forming toxin clostridium perfringens perfringolysin O: an alpha-helical to beta-sheet transition identified by fluorescence spectroscopy. Biochemistry 37:14563–14574. https://doi.org/10.1021/bi981452f

42. McCormick BA, Hofman PM, Kim J, Carnes DK, Miller SI, Madara JL. 1995. Surface attachment of salmonella typhimurium to intestinal epithelia imprints the subepithelial matrix with gradients chemotactic for neutrophils. J Cell Biol 131:1599–1608. https://doi.org/10.1083/jcb.131.6.1599

43. Mo D, Xu S, Rosa JP, Hasan S, Adams W. 2022. Dynamic python-based method provides quantitative analysis of intercellular junction organization during S. pneumoniae Infection of the respiratory epithelium. Front Cell Infect Microbiol 12:865528. https://doi.org/10.3389/fcimb.2022.865528

44. Wolfmeier H, Radecke J, Schoenauer R, Koeffel R, Babiychuk VS, Drücker P, Hathaway LJ, Mitchell TJ, Zuber B, Draeger A, Babiychuk EB. 2016. Active release of pneumolysin prepores and pores by mammalian cells undergoing a Streptococcus pneumoniae attack. Biochim Biophys Acta 1860:2498–2509. https://doi.org/10.1016/j.bbagen.2016.07.022

45. Devaux CA, Mezouar S, Mege J-L. 2019. The E-cadherin cleavage associated to pathogenic bacteria infections can favor bacterial invasion and transmigration, dysregulation of the immune response and cancer induction in humans. Front Microbiol 10:2598. https://doi.org/10.3389/fmicb.2019.02598

46. Domon H, Oda M, Maekawa T, Nagai K, Takeda W, Terao Y. 2016. Streptococcus pneumoniae disrupts pulmonary immune defence via elastase release following pneumolysin-dependent neutrophil lysis. Sci Rep 6:38013. https://doi.org/10.1038/srep38013

47. Inoshima I, Inoshima N, Wilke GA, Powers ME, Frank KM, Wang Y, Bubeck Wardenburg J. 2011. A Staphylococcus aureus pore-forming toxin subverts the activity of ADAM10 to cause lethal infection in mice. Nat Med 17:1310–1314. https://doi.org/10.1038/nm.2451

48. Aljohmani A, Opitz B, Bischoff M, Yildiz D. 2022. Pseudomonas aeruginosa triggered exosomal release of ADAM10 mediates proteolytic cleavage in Trans. Int J Mol Sci 23:1259. https://doi.org/10.3390/ijms23031259

49. Reboud E, Bouillot S, Patot S, Béganton B, Attrée I, Huber P. 2017. Pseudomonas aeruginosa ExlA and Serratia marcescens ShLA trigger cadherin cleavage by promoting calcium influx and ADAM10 activation. PLoS Pathog 13:e1006579. https://doi.org/10.1371/journal.ppat.1006579

50. Farrand AJ, LaChapelle S, Hotze EM, Johnson AE, Tweten RK. 2010. Only two amino acids are essential for cytolytic toxin recognition of cholesterol at the membrane surface. Proc Natl Acad Sci U S A 107:4341–4346. https://doi.org/10.1073/pnas.0911581107

51. Huber P. 2020. Targeting of the apical junctional complex by bacterial pathogens. Biochim Biophys Acta Biomembr 1862:183237. https://doi.org/10.1016/j.bbamem.2020.183237

52. Attali C, Durmort C, Vernet T, Di Guilmi AM. 2008. The interaction of Streptococcus pneumoniae with plasmin mediates transmigration across endothelial and epithelial monolayers by intercellular junction cleavage . Infect Immun 76:5350–5356. https://doi.org/10.1128/IAI.00184-08

53. Rubins JB, Duane PG, Clawson D, Charboneau D, Young J, Niewoehner DE. 1993. Toxicity of pneumolysin to pulmonary alveolar epithelial cells. Infect Immun 61:1352–1358. https://doi.org/10.1128/iai.61.4.1352-1358.1993

54. Veshnyakova A, Protze J, Rossa J, Blasig IE, Krause G, Piontek J. 2010. On the interaction of Clostridium perfringens enterotoxin with claudins. Toxins (Basel) 2:1336–1356. https://doi.org/10.3390/toxins2061336

55. Bourdeau RW, Malito E, Chenal A, Bishop BL, Musch MW, Villereal ML, Chang EB, Mosser EM, Rest RF, Tang WJ. 2009. Cellular functions and X-ray structure of anthrolysin O, a cholesterol-dependent cytolysin secreted by Bacillus anthracis. J Biol Chem 284:14645–14656. https://doi.org/10.1074/jbc.M807631200

56. Etxaniz A, González-Bullón D, Martín C, Ostolaza H. 2018. Membrane repair mechanisms against permeabilization by pore-forming toxins. Toxins (Basel) 10:234. https://doi.org/10.3390/toxins10060234

57. Wolfmeier H, Schoenauer R, Atanassoff AP, Neill DR, Kadioglu A, Draeger A, Babiychuk EB. 2015. Ca²⁺-dependent repair of pneumolysin pores: a new paradigm for host cellular defense against bacterial pore-forming toxins. Biochim Biophys Acta 1853:2045–2054. https://doi.org/10.1016/j.bbamcr.2014.09.005

58. Idone V, Tam C, Goss JW, Toomre D, Pypaert M, Andrews NW. 2008. Repair of injured plasma membrane by rapid Ca²⁺-dependent endocytosis. J Cell Biol 180:905–914. https://doi.org/10.1083/jcb.200708010

59. Tabusi M, Thorsdottir S, Lysandrou M, Narciso AR, Minoia M, Srambickal CV, Widengren J, Henriques-Normark B, Iovino F. 2021. Neuronal death in Pneumococcal meningitis is triggered by pneumolysin and RrgA interactions with beta-actin. PLoS Pathog 17:e1009432. https://doi.org/10.1371/journal.ppat.1009432

60. Hupp S, Förtsch C, Wippel C, Ma J, Mitchell TJ, Iliev AI. 2013. Direct transmembrane interaction between actin and the pore-competent, cholesterol-dependent cytolysin pneumolysin. J Mol Biol 425:636–646. https://doi.org/10.1016/j.jmb.2012.11.034

61. Horiuchi K, Le Gall S, Schulte M, Yamaguchi T, Reiss K, Murphy G, Toyama Y, Hartmann D, Saftig P, Blobel CP. 2007. Substrate selectivity of epidermal growth factor-receptor ligand sheddases and their regulation by phorbol esters and calcium influx. Mol Biol Cell 18:176–188. https://doi.org/10.1091/mbc.e06-01-0014

62. Pechous RD. 2017. With friends like these: the complex role of neutrophils in the progression of severe pneumonia. Front Cell Infect Microbiol 7:160. https://doi.org/10.3389/fcimb.2017.00160

63. Evans SM, Blyth DI, Wong T, Sanjar S, West MR. 2002. Decreased distribution of lung epithelial junction proteins after intratracheal antigen or lipopolysaccharide challenge: correlation with neutrophil influx and levels of BALF sE-cadherin. Am J Respir Cell Mol Biol 27:446–454. https://doi.org/10.1165/rcmb.4776

64. Balamayooran G, Batra S, Fessler MB, Happel KI, Jeyaseelan S. 2010. Mechanisms of neutrophil accumulation in the lungs against bacteria. Am J Respir Cell Mol Biol 43:5–16. https://doi.org/10.1165/rcmb.2009-0047TR

65. Dabrowski AN, Conrad C, Behrendt U, Shrivastav A, Baal N, Wienhold SM, Hackstein H, N'Guessan PD, Aly S, Reppe K, Suttorp N, Zahlten J. 2019. Peptidoglycan recognition protein 2 regulates neutrophil recruitment into the lungs after Streptococcus pneumoniae infection. Front Microbiol 10:199. https://doi.org/10.3389/fmicb.2019.00199

66. Liu CY, Liu YH, Lin SM, Yu CT, Wang CH, Lin HC, Lin CH, Kuo HP. 2003. Apoptotic neutrophils undergoing secondary necrosis induce human lung epithelial cell detachment. J Biomed Sci 10:746–756. https://doi.org/10.1159/000073962

67. Venaille TJ, Mendis AH, Phillips MJ, Thompson PJ, Robinson BW. 1995. Role of neutrophils in mediating human epithelial cell detachment from native basement membrane. J Allergy Clin Immunol 95:597–606. https://doi.org/10.1016/s0091-6749(95)70322-5

68. Yanagihara K, Fukuda Y, Seki M, Izumikawa K, Miyazaki Y, Hirakata Y, Tsukamoto K, Yamada Y, Kamihira S, Kohno S. 2007. Effects of specific neutrophil elastase inhibitor, sivelestat sodium hydrate, in murine model of severe pneumococcal pneumonia. Exp Lung Res 33:71–80. https://doi.org/10.1080/01902140701198500

69. Wilkinson TS, Conway Morris A, Kefala K, O'Kane CM, Moore NR, Booth NA, McAuley DF, Dhaliwal K, Walsh TS, Haslett C, Sallenave JM, Simpson AJ. 2012. Ventilator-associated pneumonia is characterized by excessive release of neutrophil proteases in the lung. Chest 142:1425–1432. https://doi.org/10.1378/chest.11-3273